Discrete Element modeling and analysis of shielding effects during the crushing of a grain

Wang, P., Bakhtiary, E., Ecker, S., and Arson, C.
School of Civil and Environmental Engineering
Georgia Institute of Technology, Atlanta, Georgia, USA
Christopher, T.
School of Mechanical Engineering
Georgia Institute of Technology, Atlanta, Georgia, USA
Francis, K.
School of Electrical Engineering
Georgia Institute of Technology, Atlanta, Georgia, USA

ABSTRACT: The potential for a particle to crush under one-dimensional compression is critically dependent on the coordination number of that particle. Neighboring particles decrease deviatoric forces at contacts, which reduces tensile stress and subsequent fracture propagation in the crushable particle. This phenomenon is called "shielding effect". In this paper, we model a sand particle as a spherical cluster of bonded, hexagonally packed, equally sized, non-breakable spheres with the Discrete Element Method (DEM). We use rigid walls to apply forces at the contact with neighboring particles. First, we calibrate the cluster mechanical parameters against published experimental results obtained during unconfined uniaxial compression tests. Then we propose a procedure employed in DEM to generate symmetric and random distributions of walls. We use two loading walls only: the remainder of the walls is used for passive shielding. Force-displacement curves obtained during the crushing simulations clearly show that the peak force reached when the cluster first splits increases with the number of shielding walls, which demonstrates shielding effects. The total resulting compression force applied by the walls increases linearly the coordination number. We expect that our computational method will allow the optimization of crushing in powder technology, and the prevention of crushing in geotechnical engineering.

1. INTRODUCTION

Mechanical particle crushing is used in civil engineering, powder technology and mineral industry. The most elementary crushing event is the crushing of a single particle subjected to highly compressive stresses. Single-particle compression tests, in which an individual sand grain or rock stone is vertically compressed between two horizontal platens, are often used to study crushing at the particle-scale [1-3]. Crushing depends on particle size, shape and coordination number [4-6].

Effect of particle size. Because larger particles tend to have larger internal flaws than smaller ones, particle strength decreases with particle size [7]. Hiramatsu [8] studied the stress distribution in a single particle subjected to a concentrated load by means of photoelastic experiments and mathematical analysis. They found the analytical expression of stress for spherical particles. Then based on the results of compression tests, they calculated the tensile stress in a piece of rock by

$$\sigma_f = \frac{\mathbf{0.9}\boldsymbol{F_f}}{\boldsymbol{d^2}}, \quad (1)$$

where σ_f if the tensile stress at failure, F_f is the peak compressive force applied and d is the rock particle size. Lee [9] conducted a series of compression tests of individual particles and proposed an equation to describe size effects during crushing:

$$\frac{\boldsymbol{F_f}}{\boldsymbol{d^2}} = Kd^b, \quad (2)$$

Where K is a material constant variable, and b represents the size effect.

Effect of particle shape. The shape of a particle is characterized by sphericity, roundness and

roughness[10], which have a strong influence on the initial rotation and chipping of asperities before the catastrophic crushing of the particle [6]. By idealizing particles as a hexahedron composed of two triangular pyramids, Cavarretta proposed a simplified model to calculate the vertical and horizontal displacements in the initial rotation stage. In DEM simulations (performed with PFC3D software), Cheng [2] also noticed rotation and slippage before breakage during uniaxial compression tests.

Effect of the coordination number. A high coordination number is known to prevent crushing. The mechanism can be explained by the redistribution of concentrated compression forces at particle contacts into a distributed pressure that is close to hydrostatic conditions. Hence the induced tensile stress developed inside the grain is reduced. Tsoungui [5] presented a method to combine all the contact forces applied on a particle in order to calculate the principal stresses: the loading conditions with multiple contacts is simplified into a configuration with four contacts in two principal directions, which was used to calculate the tensile stress in the particle. The tensile stress in the particle was compared with the particle strength to predict fracture propagation in the particle and crushing. Unfortunately the author did not give the solution for 3D problems. Besides, in this method the particle will never break if the two principal stresses are equal, which is obviously not practical for sand or rock particles. Lim and McDowell [3] also mentioned the importance of the coordination number in a paper that presents a model of agglomerates that they used to simulate crushable particles. But they discussed the influence of the number of particles that make the cluster, and not on the number of contacts between agglomerates. The influence of the coordination number on particle crushing is still not fully understood.

In this paper, we simulate the process of crushing of a single particle with different number of coordination numbers. We use PFC3D, a Distinct Element Method (DEM) software[11]. We model a sand particle as a spherical cluster of bonded, hexagonally packed, equally sized, non-breakable spheres. The compression forces applied by neighboring particles are accounted for by applying velocity boundary conditions to walls in contact with the cluster. The aim of our simulation is to testify the existence of shielding effect, which occurs when small particles act as a coating agent and prevent the crushing of larger particles. This paper is organized in this sequence: In the first part, we calibrate the cluster mechanical parameters against published experimental results obtained during unconfined uniaxial compression tests. In the second part, we simulate the shielding effects for a symmetric distribution of 2 to 135 walls and for a random distribution of 60 to 135 walls. Conclusions are drawn in the last part of the paper.

2. MODEL CALIBRATION

The crushable particle was modeled by a spherical cluster 1.6mm in diameter, which consisted of around 11,000 rigid (uncrushable) spheres. The normal and shear strength of the bonds between these spheres obeyed a parallel bond model, which is already implemented in PFC3D and can be seen as a cement-like substance acting as a glue between the spheres. We arranged the rigid spheres into a Hexagonal Close Packing (HCP) because it gives highest density and proved to be effective in the simulation crushable particles in PFC3D [12-14]. We note that the HCP is not symmetric, therefore the packing is denser in some directions of space, which induces anisotropic cluster mechanical properties. Therefore, we compared a vertical and a horizontal HCP (shown in Fig. 1).

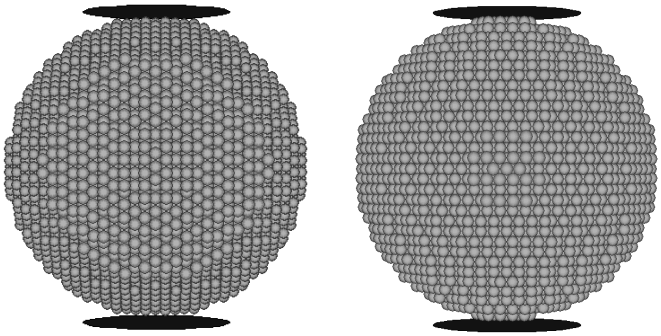

Fig. 1. Vertical and horizontal HCP of spheres used to model the crushable clusters

In order to apply the uniaxial compression force at the top and bottom of the cluster, we used disk walls (Fig. 1), which are more representative of the contact surface that develops between round particles than square walls. Disk walls had a diameter of 0.8mm. We checked that a diameter of 0.8mm size yields the same peak force at grain failure with infinite walls. This allowed us to use experimental test results obtained during the compression of individual grains between flat platens for model calibration. Wall stiffness was set to be much larger than that of spheres and bonds.

After creating the cluster and the walls, we subjected the cluster to gravity forces. Then we imposed a controlled velocity to the walls to apply the uniaxial compression force. We simulated crushing at a very low speed, in order to remain in quasi-static conditions. The intensity of forces at the walls and the number of broken bonds were monitored during the crushing simulation.

We model a sand particle similar to the one that Cil used in his experiment [13]. Experimental results used in our calibration are shown in Fig. 2. The peak compression force at failure is 146N. The size of the sand particle is between US sieves #20 (0.599 mm) and #30 (0.853 mm). For simplicity, we used the average value, i.e. 0.729mm.

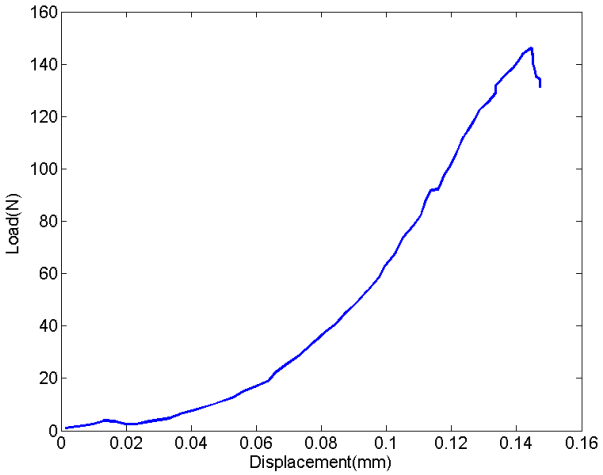

Fig. 2. Load-displacement curve obtained during the experiment of a uniaxial compression test performed on a crushable sand grain [13]

In order to calculate the peak force of different sizes with Eq.(2), we had to determine the size effect parameter b. Lee's compression tests of individual particles of Leighton Buzzard sand, oolitic limestone and carboniferous limestone revealed that the size effect parameters in Eq.(2) were -0.357, -0.343 and -0.420, respectively [4, 9]. To our best knowledge, more precise experimental data does not exist in the literature. Therefore, we assumed that b was between -0.343 and -0.420. According to Eq.(2), by computing the ratio of forces and cancelling K, the peak compression force for the same sand particle with a diameter of 1.6mm should between 506N and 531N. The calibration process is done by continuously adjusting parameters, i.e. normal and shear parallel bond strength and stiffness, to best fit the peak force and the shape of the displacement-force. A summary of final parameters used in the simulation is reported in Table 1, and the corresponding calibration results are shown in Fig. 4.

Table 1. Parameters used in DEM simulation

Input parameter	Value
Diameter of cluster: mm	1.6
Diameter of sphere: mm	3.2×10^{-2}
Density of sphere: kg/m^3	3581
Normal and shear stiffness of each sphere: N/m	1×10^{6}
Normal and shear bond strength: MPa	170
Normal stiffness of parallel bond: N/m^3	3×10^{14}
Shear stiffness of parallel bond: N/m^3	1×10^{14}
Frictional coefficient of sphere	0.5

The pattern of Load-Displacement curve is similar to that in the experiment. The model captures and the breakage of the cluster into several fragments (Fig. 3) and the peak force when this catastrophic collapse occurs (Fig. 4). It is interesting to find that an initial peak is obtained with the horizontal HCP (point A in Fig. 4), and not with the vertical HCP. We also noted that the horizontal HCP cluster was rotating during the simulations. Similar initial peak forces and rotations were obtained and analyzed by other searchers [2, 15]. Rotation is interpreted as the minimization of the potential energy of the cluster, which gets closer to a stable equilibrium position. Despite this difference of curve shape between the two packing tested, the peak forces only exhibited a 4% difference: we obtained peak forces of 509N (for the vertical HCP) and 489N (for the horizontal HCP), which falls close to the range of 506N and 531N expected. We also note that the final number of broken bonds is the same for both packings.

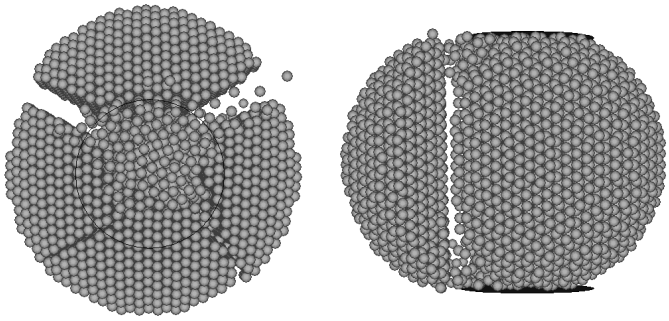

(a) (b)

Fig. 3. (a) Plan view of vertical HCP cluster after the first breakage; (b) front view of the cluster after the first breakage

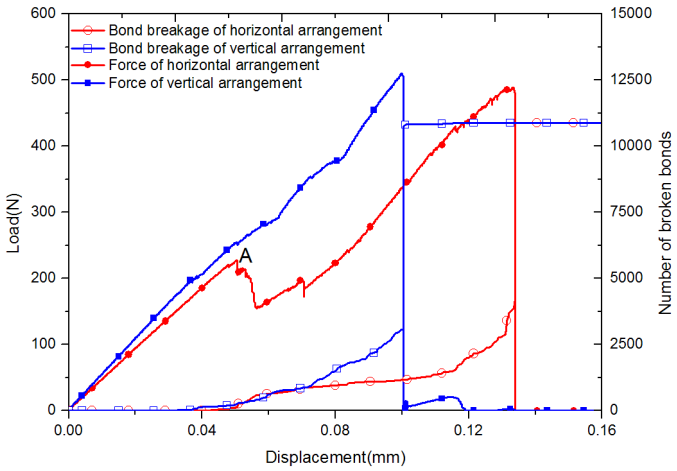

Fig. 4. Load-displacement relationships and number of broken bonds during the calibration simulations, for both vertical and horizontal HCP cluster models

3. SHIELDING EFFECT

We used the calibrated cluster model to simulate shielding effects with an increased number of contact walls. We assumed that crushing was controlled by the two largest particles surrounding the cluster, and that the other neighboring particles acted as a passive shield (in the form of a confining stress). Therefore, we applied the loading force through two walls only. The other walls were fixed during the simulation. In the following, the top and bottom walls (subjected to loading forces) are called *loading walls*, and the surrounding walls are called *shielding walls*. In order to avoid the initial cluster rotation noted earlier, we used the vertical HCP model.

3.1. *Numerical Procedure*

The shielding model is generated in four steps:

1. *Generate the cluster and loading walls*. This step is similar to that used for the calibration simulations presented in Section 2.

2. *Generate shielding walls*. Shielding walls are small disk walls that are tangent to the cluster. The radius of the shielding walls was 0.1mm, about 3 times the radius of the rigid spheres inside the cluster, in order to ensure a good distribution of stresses at the contacts. During the crushing process, shielding walls redistribute contact forces, which reduces concentrated compressive forces at the contacts and tensile stress in the cluster. In order to avoid significant unbalanced forces due to the non-uniform distribution of shielding walls, shielding walls were placed according to a symmetric distribution around the cluster for low coordination numbers, up to 60 walls. Above 60 walls, shielding effects produced by both symmetric and random wall distributions were simulated. The procedure adopted to generate symmetric wall distributions is illustrated in Fig. 5 andTable 2. Random wall distributions were generated by random point picking, with normal vectors pointing towards the origin [16]. Any shielding wall that has overlap with other ones is deleted. Gravity was applied after all the walls were created.

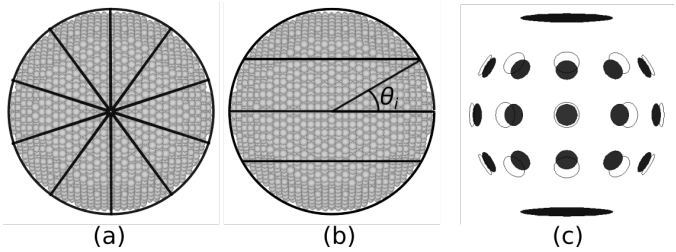

Fig. 5. Procedure to generate a symmetric distribution 30 walls (10×3): (a) divide the cluster into ten "slices" along vertical lines (plan view); (b) choose an orientation θ_i (in reference to the horizontal) to find the position of two circles of same diameter on the upper and lower hemispheres; (c) generate walls at the intersections of these lines.

3. A*pply shielding forces*. A very small velocity was then given to all the shielding walls, in order to make them move towards the center of the cluster, which generated the desired shielding (confining) forces in the cluster. The number of broken parallel bonds in the cluster was counted after each cycle, and the wall velocity was reset to zero after the first bond breakage. By doing so, strong shielding forces were imposed to the cluster.

4. *Crush the cluster.* The two loading walls were displaced slowly towards the particle, while keeping the shielding walls at a fixed position. Forces developed on the loading walls were monitored.

Table 2. Geometric parameters of the symmetric distribution of shielding walls. The number of walls $N=N_1xN_2$ is the product of the number of wall centroids in a plane (N_1) by the number of horizontal planes containing wall centroids (N_2). θ_i is the orientation of the walls in reference to the horizontal.

Nb. of walls	θ_i (°)	Nb. of walls	θ_i (°)
4×1=4	0	10×5=50	0, 30,45
8×1=8	0	8×7=56	0, 30,45,60
10×1=10	0	12×5=60	0, 30,45
12×1=12	0	10×7=70	0, 30,45,60
15×1=15	0	8×9=72	0,15,30,45,60
6×3=18	0, 30	15×5=75	0,30,45
8×3=24	0, 30	12×7=84	0,30,45,60
10×3=30	0, 30	10×9=90	0,15,30,45,60
12×3=36	0, 30	15×7=105	0,30,45,60
8×5=40	0,30,45	12×9=108	0,15,30,45,60
15×3=45	0, 30	15×9=135	0,15,30,45,60

3.2. *Simulation Results*

Fig. 6 shows selected force-displacement curves that we obtained in the simulations. It is clear that the magnitudes of the peak force and the wall displacement at the first occurrence of particle fragmentation increases with the number of shielding walls. The sharp decrease of the reaction force at the contact with the loading walls is observed in all shielding simulations. By contrast with experimental load-displacement curves that exhibit a concave shape, the slope of the load-displacement curves obtained numerically was approximately constant before cluster crushing. This is because linear elastic law is used both in contact model and parallel bond model before breakage.

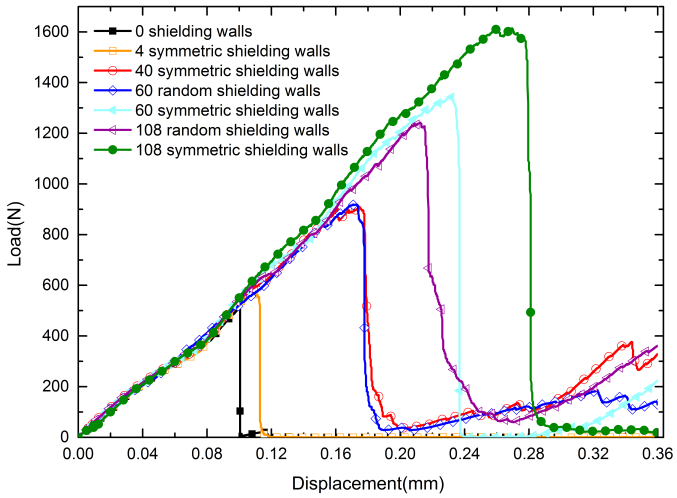

Fig. 6. Force-displacement curves obtained in the compression tests with account of shielding effects

The relationship between the peak compression force and the number of shielding walls is illustrated in Fig. 7, which shows obvious shielding effects for both symmetric and random distributions of walls. The peak force reached at the first cluster fragmentation is approximately proportional to the number of shielding walls with the slope of 10.18 and 7.56, respectively. In most cases, the peak force for a symmetric wall distribution is larger than that for a random wall distribution. This can be explained by the fact that symmetrically distributed walls can more effectively redistribute stresses around the cluster, which reduces stress concentrations inside the cluster and prevents the propagation of micro fractures in the cluster (by bond breakage). From the simulation results obtained for randomly distributed walls, we estimate that at least 80 walls are needed to double the peak forces.

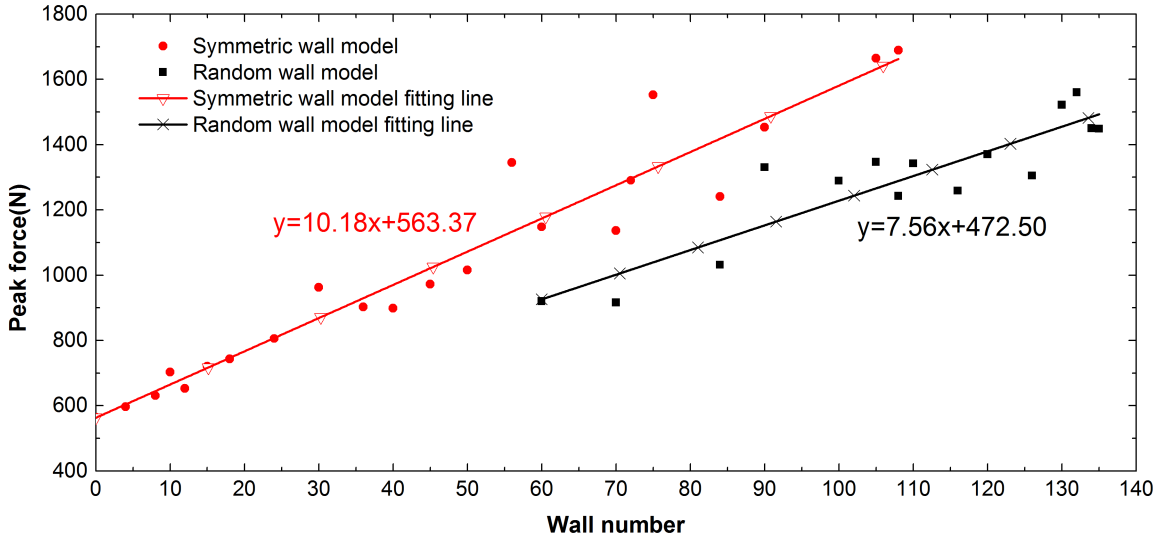

Fig. 7. Relationship between peak compression force at the first occurrence of failure during the compression tests, and the number of shielding walls used in the simulations (coordination number of the cluster).

4. CONCLUSIONS

In this paper, we used a Discrete Element Method to study the influence of the coordination number of a crushable particle on shielding effects. We calibrated the mechanical parameters of a cluster made of hexagonally packed bonded spheres against published experimental results obtained during unconfined uniaxial compression tests. We hypothesized that shielding effects that prevent crushing are due to the redistribution of contact forces towards a quasi-hydrostatic stress distribution: lower stress concentrations prevents fracture propagation. In order to test this assumption, we modeled neighboring particles around the cluster by rigid walls acting in compression ('loading walls') or in confinement ('shielding walls'). We used both symmetric and random wall distributions around the cluster. Simulations confirm that the peak force increases with the number of shielding walls, i.e., with the coordination number of the crushable particle. We found that the peak force reached when the cluster is split for the first time is approximately proportional to the coordination number. Symmetric wall distributions exhibited higher shielding effects. Random wall distributions generate less uniform stress distributions, which could explain the difference between the two wall arrangements. More work is needed to predict the slope coefficient in the linear relationship that links the peak force to the coordination number. But we can reasonably guess that the maximum peak force of a particle is determined by the number it can accommodate at the surface.

In future work, we will verify the assumptions we made here to explain shielding effects that prevent crushing by simulating the one-dimensional compression of a granular assembly made of crushable cluster surrounded by rigid spheres of various sizes. We aim to gain a better understanding of the interactions between shielding particles, and of the re-organization of the fabric of granular assemblies subject to crushing. Research outcomes are expected to help optimizing rock fragmentation during excavation works, and designing materials that can be used as crushing shields in civil engineering (e.g., ballast).

ACKNOWLEDGEMENTS

The authors acknowledge the financial support from the American Association of Railways and the institutional assistance of Vertically Integrated Program on Energy Geotechnology at the Georgia Institute of Technology.

REFERENCES

1. Cavarretta, I, O'sullivan, C. 2012. The mechanics of rigid irregular particles subject

to uniaxial compression. *Geotechnique.* 62(8):681-692.
2. Cheng, YP, Nakata, Y, Bolton, MD. 2003. Discrete element simulation of crushable soil. *Geotechnique.* 53(7):633-641.
3. Mcdowell, GR, Lim, WL. 2007. The importance of coordination number in using agglomerates to simulate crushable particles in the discrete element method. *Geotechnique.* 57(8):701-705.
4. Mcdowell, GR, Bolton, MD. 1998. On the micromechanics of crushable aggregates. *Geotechnique.* 48(5):667-679.
5. Tsoungui, O, Vallet, D, Charmet, JC. 1999. Numerical model of crushing of grains inside two-dimensional granular materials. *Powder Technol.* 105(1-3):190-198.
6. Cavarretta, I. 2009. *The influence of particle characteristics on the engineering behaviour of granular materials*. London: Imperial College.
7. Lim, WL. 2004. *Mechanics of railway ballast behaviour*. Nottingham: University of Nottingham.
8. Hiramatsu, Y, Oka, Y. 1966. Determination of the tensile strength of rock by a compression test of an irregular test piece. *International Journal of Rock Mechanics and Mining Sciences & Geomechanics Abstracts.* 3(2):89-90.
9. Lee, DM. 1992. *The Angles of Friction of Granular Fills*. Cambridge: University of Cambridge.
10. Santamarina, J, Cho, G. 2004. Soil behaviour: The role of particle shape. In: *Advances in geotechnical engineering: The skempton conference: 2004*: Thomas Telford; 2004: 604-617.
11. Potyondy, DO, Cundall, PA. 2004. A bonded-particle model for rock. *Int J Rock Mech Min.* 41(8):1329-1364.
12. Robertson, D. 2000. *Numerical simulations of crushable aggregates*. Ph. D. dissertation, University of Cambridge.
13. Cil, MB, Alshibli, KA. 2014. 3D Modeling of Sand Particle Fracture Using Discrete Element Method and Synchrotron Micro-Tomography Images. *In Geo-Congress 2014 Technical Papers@ sGeo-characterization and Modeling for Sustainability,* 2014, Atlanta.
14. Mcdowell, GR, Harireche, O. 2002. Discrete element modelling of soil particle fracture. *Geotechnique.* 52(2):131-135.
15. Lu, M, Mcdowell, GR. 2006. The importance of modelling ballast particle shape in the discrete element method. *Granul Matter.* 9(1-2):69-80.
16. Marsaglia, G. 1972. Choosing a point from the surface of a sphere. *The Annals of Mathematical Statistics.* 43(2):645-646.